tvst

Article

Imaging of Therapeutic Effects of Anti-Vascular Endothelial Growth Factor Inhibitors by Optical Coherence Tomography Angiography in a Rat Model

Johanna H. Meyer[1], Janine Marx[1], Claudine Strack[1], Frank G. Holz[1], and Steffen Schmitz-Valckenberg[1,2]

[1] Department of Ophthalmology, University of Bonn, Bonn, Germany
[2] John A. Moran Eye Center, University of Utah, Salt Lake City, UT, USA

Correspondence: Johanna H. Meyer, Department of Ophthalmology, Bonn, Germany, Ernst-Abbe-Str. 2, 53127 Bonn, Germany. e-mail: Johanna.Meyer@uni-bonn.de

Received: March 13, 2020
Accepted: April 24, 2020
Published: June 25, 2020

Keywords: OCT angiography; laser-induced CNV; aflibercept; AF564; rat

Citation: Meyer JH, Marx J, Strack C, Holz FG, Schmitz-Valckenberg S. Imaging of therapeutic effects of anti-vascular endothelial growth factor inhibitors by optical coherence tomography angiography in a rat model. Trans Vis Sci Tech. 2020;9(7):29, https://doi.org/10.1167/tvst.9.7.29

Purpose: The aim of the study was to investigate optical coherence tomography angiography (OCTA) as a high-resolution in vivo imaging modality for monitoring therapeutic response to different vascular endothelial growth factor inhibitors in the rat model of laser-induced choroidal neovascularization (CNV). Further, OCTA findings were compared with fluorescein angiography (FA) and fluorescence microscopy.

Methods: Laser treatment at day (D)0 was followed by intravitreal injection of aflibercept, AF564, and NaCl in dark agouti rats. Imaging with OCTA and FA was performed at D2, D7, D14, and D21. OCTA was compared to FA as well as confocal imaged flat mounts and analysis included quantification of CNV area, pixel intensity, vessel density, and number of vessel junctions.

Results: Within laser lesions, neovascularization were visible especially in deeper retinal layers on OCTA, but not on FA images. Using OCTA, mean CNV area (D21) at the level of the outer nuclear layer (ONL) was 0.017 mm^2 following aflibercept administration, 0.016 mm^2 following AF564 and 0.026 mm^2 following NaCl injection ($P = 0.04$ and $P = 0.03$). Similar differences between treatment groups were determined by FA and histology, although the overall CNV area was always larger on FA due to dye leakage ($P \leq 0.0001$, all layers).

Conclusions: Compared to FA, OCTA imaging allows for a more precise and quantitative analysis of new blood vessel formation and therapeutic response to vascular endothelial growth factor (VEGF)-inhibitors, whereas it does not permit assessment of leakage.

Translational Relevance: These findings suggest that OCTA may be particularly useful for the investigation of new treatment targets in the animal model.

Introduction

Choroidal neovascularization (CNV) is the hallmark of neovascular age-related macular degeneration (AMD), which represents the leading cause of blindness in industrialized nations. The neovascular phenotype of the disease is characterized by formation and invasion of abnormal blood vessels at the posterior pole that penetrate through Bruch's membrane.[1] CNV is typically associated with hyperpermeability and thus exudation of fluid, as well as hemorrhage and subsequent fibrosis, resulting in severe damage to neuronal tissue and, thus, vision loss. Enhanced expression of the angiogenic cytokine vascular endothelial growth factor (VEGF) has been validated in patients with CNV and anti-VEGF therapy has been established as the standard of care for CNV.[2,3] Currently, the humanized monoclonal anti-VEGF antibody bevacizumab, the Fab fragment ranibizumab, the VEGF-A receptor fusion protein aflibercept, and the single-chain variable fragment broculizumab are applied intravitreally for the treatment of neovascular AMD.[4–7] Thereby, the process of

Copyright 2020 The Authors

This work is licensed under a Creative Commons Attribution-NonCommercial-NoDerivatives 4.0 International License.

CNV and vascular leakage can be targeted. Despite this progress, a significant proportion of patients with AMD will still experience significant vision impairment.[8,9] Therefore, there it is still an unmet need to better understand the underlying pathogenesis of CNV and to identify and develop more efficacious therapeutic targets with longer duration of the therapeutic effects.

The development of the imaging modality optical coherence tomography angiography (OCTA) allows for the in vivo visualization of the blood flow in retinal and choroidal vessels at high resolution.[10,11] In addition to being a noninvasive modality, the key advantage of OCTA is the ability to perform a three-dimensional analysis of the vasculature at the posterior pole.[10] The main principle of OCTA is the algorithm-based detection of blood motion contrasts by comparing the static and dynamic signal properties between consecutive OCT-B-scans.[12] OCTA has been proven to be beneficial in clinical routine and visualize disease structures in detail as well as high accuracy in many diseases, including AMD, diabetic retinopathy, glaucoma, uveitis, and retinal vascular occlusions.[11,13] In parallel to its use in humans, advances in noninvasive retinal imaging techniques also open the door for new and innovative experimental animal research, including the application of OCTA in addition to other in vivo imaging modalities, such as fundus camera photography, confocal scanning laser ophthalmoscopy (cSLO), and structural optical coherence tomography (OCT).[14–19] For example, the efficacy of new therapeutic target molecules for neovascular AMD can be tested in the well-described laser-induced CNV model. Hereby, treatment responses can be determined longitudinally in the same animal by serial in vivo imaging.[20] In this context, progression of CNV after the application of VEGF inhibitors in the laser-induced CNV model has rarely been examined using commercial OCTA devices.[21] Furthermore, there is a lack of detailed analyses by OCTA particularly in comparison to conventional fluorescein angiography (FA) or ex vivo preparations.[22,23]

The aim of the current study was to investigate high resolution in vivo OCTA imaging in the rat model of laser-induced CNV for monitoring therapeutic response to two different VEGF inhibitors. In addition, OCTA observations were compared with conventional FA at different time points in the same animal. Finally, retinal and retinal pigment epithelium (RPE)/choroidal/scleral flat mount preparations were analyzed by confocal fluorescence microscopy and compared with the in vivo findings.

Materials and Methods

Animals

Experiments were performed with adult Dark Agouti rats ($n = 35$; Janvier Labs, Rennes, France), each weighing 200 to 250 g. All animal procedures were conformed with the Association for Research in Vision and Ophthalmology statement for the Use of Animals in Ophthalmic and Vision Research and approved by the local authorities (local ethics committee "Landesamt für Natur, Umwelt und Verbraucherschutz Nordrhein-Westfalen" in Germany). Rats were fed with normal rodent chow and supplied with water ad libitum. For all procedures, they were anesthetized by intraperitoneal injection of a ketamine (60 mg/kg, bela-pharma; GmbH & Co. KG, Vechta, Germany) and medetomidine hydrochloride (0.5 mg/kg; Orion Pharma, Espoo, Finland) mixture as previously described.[24] Supplemental anesthesia was administered intraperitoneally as needed and anesthesia of rats was reversed by intraperitoneal injection of a 20% atipamezole (1 ml/kg; Orion Pharma) solution at the end of the experiment. Animals received a topical administration of 0.5% tropicamide (Mydriaticum Stulln, Pharma Stulln, Stulln, Germany) eye drops for pupillary dilation of both eyes before in vivo imaging as well as laser treatment. For all procedures, rats were kept on a heating pad (37°C) to maintain the body temperature. Imaging was followed by topical administration of Corneregel (Bausch & Lomb, Berlin, Germany) and animals were returned to their housing after full recovery from anesthesia.

Laser Treatment and Drug Administration

As previously described, retinal laser lesions were generated at day 0 (D0) to induce CNV formation.[15,25] In brief, the pupils were dilated with 0.5% tropicamide (Mydriaticum Stulln, Pharma Stulln, Stulln, Germany) and 10% phenylephrine hydrochloride (URSAPharm, Saarbrücken, Germany) before laser treatment. In all eyes, three to four laser lesions (excitation: 514 nm, pulse duration: 0.1 seconds, laser power: 150 mW and spot size: 100 µm) were placed around the optic nerve head and between the major retinal vessels in each eye using a slit-lamp delivery system combined with an argon laser (Novus 2000; Coherent, Dieburg, Germany). Successful disruption of Bruch's membrane was confirmed by formation of a bubble at the site of laser application immediately visualized with the slit lamp. Lesions with significant subretinal hemorrhage

or without a bubble formation following the laser treatment were excluded ($n = 3$).

To investigate the visualization of new vessel formation by OCTA and FA under the therapeutic intervention with VEGF inhibitors, rats were randomly assigned to treatment and control groups. In the treatment group, aflibercept (a recombinant humanized anti-VEGF fusion protein, Bayer Pharma AG, Berlin, Germany) and AF564 (a rat-specific polyclonal anti-VEGF antibody; R&D Systems, Minneapolis, MN; dissolved in NaCl) were used.[26] AF564 is a widely used polyclonal goat immunoglobulin G (IgG) that has proven to be a potent inhibitor of $VEGF_{164}$.[20,27–29] In direct enzyme-linked immunosorbent assays (ELISAs), approximately 20% cross-reactivity with recombinant human (rh) $VEGF_{165}$ and $rhVEGF_{121}$ is observed and < 2% cross-reactivity with rhVEGF-B, recombinant mouse (rm) VEGF-B, rhVEGF-C, rhVEGF-D, and rmVEGF-D is observed.[30] In addition, NaCl (Fresenius Kabi Deutschland GmbH, Bad Homburg, Germany) served as control. Immediately (2–10 minutes) following the laser treatment (D0), a 5 µl intravitreal injection of NaCl (n = 9 animals), aflibercept (10 µg/µl; $n = 9$), and AF564 (5 µg/µl; $n = 10$) was administered into both eyes using a microliter syringe (Hamilton Company, Bonaduz, Switzerland) with a 30-gauge needle under a microscope.[26] By holding the conjunctivae with fine forceps, eyes were slightly protruded and stabilized. Each eye received a single injection and, for this purpose, the needle was inserted approximately 2 mm from the limbus with a depth of approximately 3 to 5 mm. The needle was kept in place for 30 seconds to prevent the reflux of solution when the needle was removed. The injections were always administered by the same person.

OCT Angiography

In vivo imaging in rats was performed at days 2, 7, 14, and 21 following the initial laser treatment. Anesthetized animals were placed on a customized platform in front of the camera lens and a 55° lens was used for both cSLO and OCTA imaging. For OCTA, an OCTA device (Spectralis prototype; Heidelberg Engineering GmbH, Heidelberg, Germany, software version SP-X1601) was utilized in the high resolution mode as described previously.[22,31] Rigid rat contact lenses (Cantor & Nissel Limited, Brackley, Northamptonshire, UK) were applied during OCTA to prevent corneal dehydration and cataract formation.[22] For OCTA imaging, a standardized focus setting of + 17.25 diopter was selected for all eyes and accordingly the length of the OCT reference arm was adjusted to the rat eye in the Spectralis OCT-debug window reaching 29,000 until 31,000 µm. The size of the scan field was adjusted by using one of three different volumes (20° × 20°, 25° × 25°, and 25° × 55°) with 350 until 651 horizontal OCTA-B-scans (depending on the area involvement of the applied laser spots). For the calculation of one B-scan, 25 sequential frames were used and the distance between 2 single B-scans was set to 11 µm.

For analysis of OCTA images (Fig. 1 and Supplementary Fig. S1), seven retinal and choroidal layers were segmented: superficial vascular plexus (SVP), intermediate vascular plexus (IVP), deep vascular plexus (DVP), outer nuclear layer (ONL), ellipsoid zone (EZ; containing the inner and outer segments of the photoreceptors), inner choroid (IC), and outer choroid (OC).[22,31] OCTA segmentation was performed standardized and semimanually by automatically selecting the inner limiting membrane (ILM) followed by manually shifting segmentation of all seven layers (Fig. 1 and Supplementary Fig. S1). The superficial plexus was segmented from 30 µm to 60 µm below the ILM, followed by the intermediate plexus (30 µm), the deep plexus (30 µm), the ONL (60 µm), and the EZ (40 µm). Below the RPE, the IC layer (30 µm) and the OC layer (80 µm) were segmented (Supplementary Fig. S1).[22] OCTA en-face images were compared to cSLO images obtained by conventional FA.

Fluorescein Angiography Using Confocal Scanning Laser Ophthalmoscopy

Conventional FA of the CNV lesions was conducted using a cSLO (Heidelberg Retina Angiograph 2 HRA 2; Heidelberg Engineering GmbH) in a single and standardized session.[22,31] Anesthetized animals were placed on a custom mounting platform in front of the 55° camera lens.[24,31] Lubricating eye drops (Oculotect fluid 50 mg/mL; Novartis Pharma, Nürnberg, Germany) were used during FA imaging to prevent corneal dehydration and cataract formation. Each animal underwent serial intravenous injection of 10% fluorescein solution (Fluorescein Alcon; Alcon Pharma GmbH, Freiburg, Germany) with identical concentration followed by in vivo fluorescence imaging at days 2, 7, 14, and 21 following initial laser treatment.[22] A mean image of a series of single images (15 frames) was achieved to improve the signal-to-noise ratio and to enhance image contrast. For FA, 10% fluorescein dye (dose: 50 mg/kg) was injected intravenously (0.2 mL) and laser power was set at 20% and the detector sensitivity at 50% in the high-resolution mode. Immediately following the dye injection, the topographic uptake

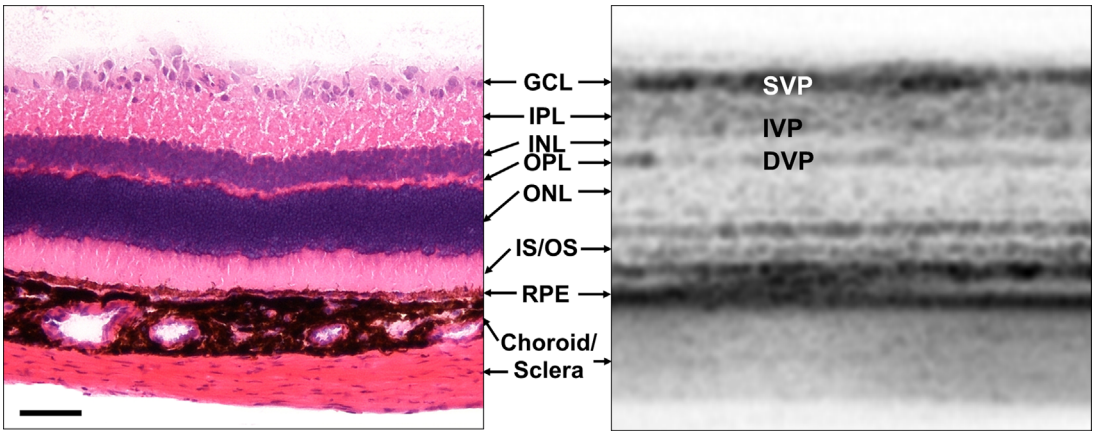

Figure 1. Morphology and vascular plexus of the (rat) retina. The retinal capillary network consists of three different plexus: superficial vascular plexus (SVP), intermediate vascular plexus (IVP), and deep vascular plexus (DVP). The different morphological layers and retinal vascular plexus are indicated in a H&E stained cross section and an OCT-B scan of untreated rat eyes. GCL, ganglion cell layer; INL, inner nuclear layer; IPL, =inner plexiform layer; IS/OS, inner and outer segment; ONL, outer nuclear layer; OPL, outer plexiform layer; RPE, retinal pigment epithelium. Scale bar: 100 µm.

was recorded using different focus settings (from + 18, + 16, + 15, + 14, + 13, + 12, + 11, + 10, + 9, + 8, + 7, + 6, + 5, + 4, + 3, + 2, + 1, 0, −4, and −8 diopter). The confocal approach allows for the acquisition of sectional scans through the rodent retina and investigates the depth location of fluorescent signals.[22,32] Timing began immediately after the fluorescein injection and ended 10 minutes following the intravenous dye injection. In order to compare different fluorescence intensities, standardized focus settings of + 14 (SVP), + 10 (IVP), + 6 (DVP), + 3 (ONL), 0 (EZ), −4 (IC), and −8 (OC) diopter were defined.

In Vivo Image Analysis

The CNV area (or laser lesion size), in both image modalities (OCTA and FA) and blinded to both treatment assignment and day, was quantified using the automated measuring tool provided by the system manufacturer (Heidelberg Eye Explorer, version 1.9.10.0, 2014; Heidelberg Engineering GmbH) by selecting the area of CNV for each laser spot (NaCl: $n = 30$; aflibercept: $n = 19$; and AF564: $n = 37$). For each lesion, CNV area was measured in the seven defined layers and at all time points.[22] The laser lesion size was averaged for all examined animals and treatment groups to examine the overall CNV area (and SD). For scaling in the metric system, area size of CNV lesions was calculated in relation to the size of the optic nerve head as previously described, assuming a standard optic disc size of 0.041 mm^2.[22,33] The reduction of the laser spot size was determined with respect to the size of the laser spots at D2 of the NaCl control group for OCTA and FA images for each tested treatment group, day, and layer.

To further analyze the relationship between the anti-VEGF treatment and degree of angiographic leakage, dye leakage of each CNV lesion was estimated with an adapted CNV grading score (Supplementary Fig. S2).[14,34,35] Two independent investigators evaluated the fluorescein angiograms in a blinded manner in a single session. Therefore, CNV formation was evaluated according to the presence or absence of dye leakage with a grading score from 0 to 3. Lesions were graded as follows: no leakage (score 0), minimum leakage or a staining of tissue with no leakage without progression in size and intensity (score 1), small but evident leakage with an increase in intensity but not in size (score 2), and large evident leakage with increase in intensity and size (score 3).[34,35] Only lesions with grade 3 leakage were considered as an active lesion. If the two masked graders did not agree for a particular lesion, the higher score was used in the analysis.

For the more detailed quantitative analysis of angiographic leakage between the treatment groups, the pixel intensity was calculated within the laser spots using Photoshop CS5 software (Adobe Systems, Inc., San Jose, CA). The overall fluorescence intensity (background signal) was assessed accordingly from a randomly selected well-illuminated choroidal area outside the laser lesions, which did not contain major blood vessels, followed by subtracting the averaged background pixel intensity and mean gray value from the laser spot values.[26]

In addition, the retinal vascular network was analyzed by AngioTool software (Center for Cancer

Research, version 0.6a, 64 bits, October 2014)[36] as a plugin of Fiji (ImageJ version 1.48; Wayne Rasband, National Institute of Health, Bethesda, USA).[17,22,37] The OCTA and FA images of the SVP, IVP, and DVP for all treatment groups were transformed to equal sizes by Fiji covering the area of laser lesions before the assessment of the retinal vascular plexus using AngioTool. The average number of visualized retinal vessels was calculated as vessel density indicating the percentage of area occupied by vessels inside the explant area in OCTA and FA images.[36] Furthermore, the number of vessel junctions in the area of CNV in the SVP, IVP and DVP in OCTA, and FA images were analyzed separately for the three treatment groups.

Ex Vivo Measures and Histology

At D21, following the in vivo imaging by OCTA and FA, anti-VEGF (aflibercept: $n = 10$ and AF564: $n = 10$), and NaCl control (NaCl: $n = 9$) animals were euthanized by applying 100% carbonic acid gas. Eyes were immediately enucleated and processed for retinal and RPE/choroidal/scleral flat mount preparation or frozen sections and examined by fluorescence microscopy.[22] For flat mount preparation, following enucleation and fixation for 90 minutes in fresh 4% paraformaldehyde (PFA), the anterior part of the eye was removed and the retina as well as the RPE/choroidal/scleral complex were separated. The eye cups were washed several times with phosphate-buffered saline (PBS), then blocked with immunocytochemistry (ICC) buffer containing 0.5% bovine serum albumin (BSA), 0.2% Tween20, and 0.1% Triton X-100 (all: PAA Laboratories GmbH, Cölbe, Germany) in PBS for 2 × 15 minutes. Flat mount sections were then incubated with a 1:100 dilution of isolectin B4 (IB4, I21411, Alexa488 conjugated; Life Technologies, Eugene, OR) for 2 hours at room temperature on a shaker. After four washing steps with PBS, four to six relaxing radial incisions were made and the retinal and RPE/choroidal/scleral segments were mounted on a glass slide with Shandon Immu-Mount Medium (Thermo Scientific, Fisher, UK) with the photoreceptor side down. An upright Leica TCS SP8 laser scanning confocal microscope with an acousto-optical beam splitter (Leica TCS SP8; Leica Mikrosysteme Vertrieb GmbH, Wetzlar, Germany) using a 10× objective and a solid-state laser for 488 nm was used for sample observation and image acquisition. An image z-stack containing the region of interest was collected and ex vivo CNV area was measured in retinal and RPE/choroidal/scleral flat mounts using ImageJ software. The mean CNV area was calculated and compared with OCTA and FA results at D21. Data were excluded if tissue damage occurred in the CNV area during flat mount processing.

For additional light microscopic examination of frozen sections (see Fig. 1), healthy and untreated eyes ($n = 8$) were processed by embedding in OCT medium (Tissue Tek, Sakura Finetek Europe B.V., Alphen aan den Rijn, The Netherlands) on dry ice and stored at −80°C until needed. Frozen sections (see Fig. 1) of 10 µm were mounted on a glass slide, fixed with 100% methanol and stained with hematoxylin and eosin (H&E). The H&E stains were investigated at 20× magnification with a light microscope (Olympus BX50; Olympus, Hamburg, Germany).

Statistical Analysis

Statistical analyses were performed using the SPSS software package Statistics 25 (SPSS Inc., Chicago, IL). All results were expressed as mean values ± SD. Comparison of mean CNV area between the three different treatment groups in the ONL and EZ was performed using the Kruskal–Wallis test, followed by a Wilcoxon test. In addition, also the pixel intensity within the laser lesions was statistically analyzed with the Wilcoxon test and the χ^2 test was used for the analysis of the grading score in FA images. Statistical analysis of vessel density and number of vessel junctions within the laser spot were performed using the Wilcoxon test. Comparison of mean CNV area between OCTA and histology as well as FA and histology was performed using Wilcoxon test. Comparison of mean CNV area (in mm^2) between OCTA and FA was performed using the Wilcoxon test. The P values < 0.05 were considered as statistically significant and significance levels are indicated using * for $P \leq 0.05$, ** for $P \leq 0.01$, and *** for $P \leq 0.001$.

Results

In Vivo Imaging

Noninvasive and high-resolution imaging using OCTA of the different retinal and choroidal vascular structures in vivo of the rodent eye was achieved in the NaCl (Supplementary Fig. S3), aflibercept (Supplementary Fig. S4), and AF564 (Supplementary Fig. S5) groups at any time point (Fig. 2). In general, three-dimensional OCTA imaging showed a more detailed representation of the retinal and choroidal blood vessel structures compared with conventional FA. Thus, the precise detection of the vasculature network in the rat eye and focal laser lesions (see

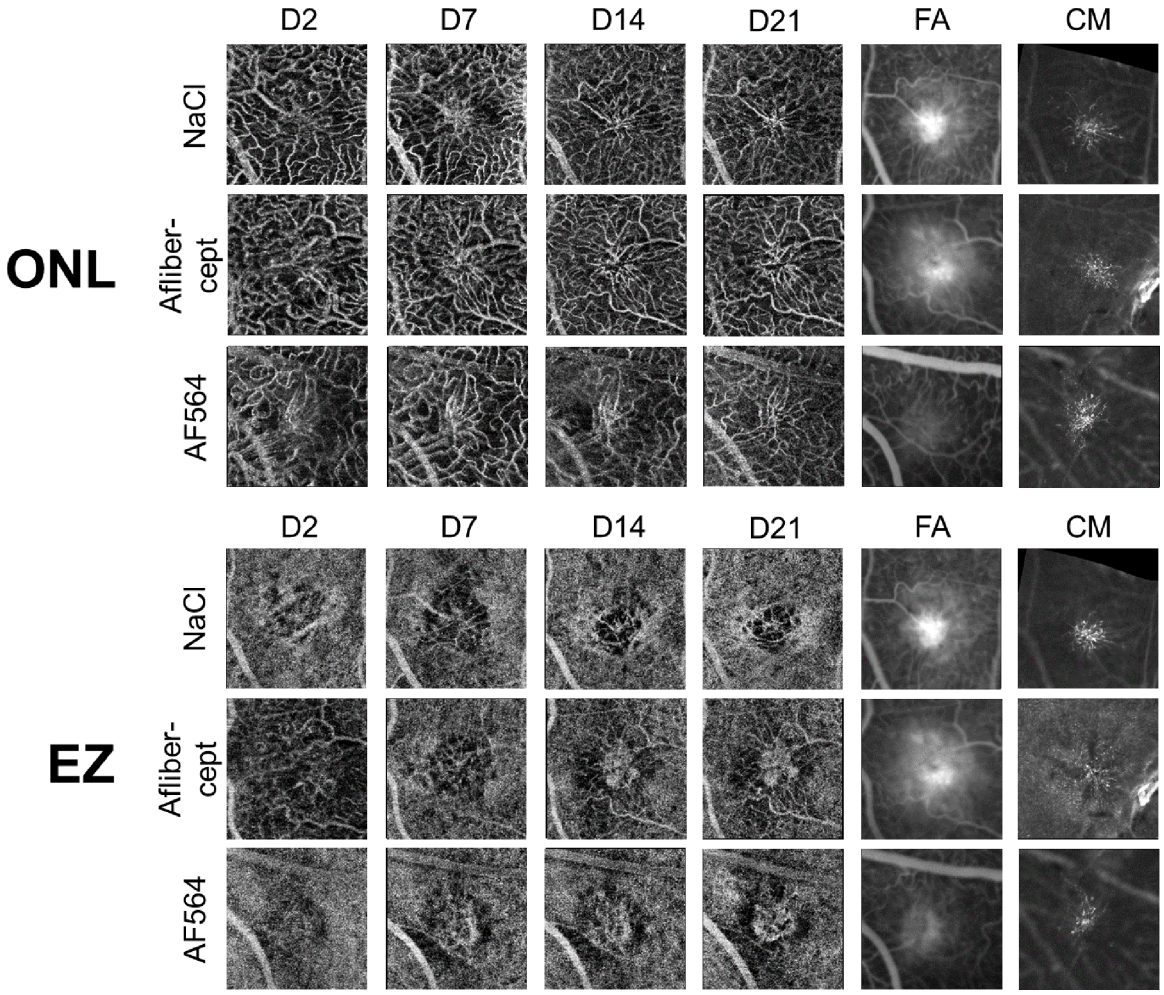

Figure 2. Visualization of laser lesions in ONL and EZ by OCTA (D2–D21), FA, and confocal microscopy (CM). In vivo imaging following the intravitreal injection of NaCl, aflibercept, and AF564 was conducted over time and time points are indicated above the respective OCTA images (first four columns; D = day following initial laser treatment and intravitreal injection). At D2, signs of edema and swelling of the tissue as effect of the laser treatment were visualized but no new blood vessels were observed in OCTA images. Early formation of neovascular vessels was identified at D7 in the ONL and EZ. A subtle capillary network in the EZ was detected 21 days following the initial laser treatment in all groups, but particularly in NaCl treated eyes. In FA images (at D21), neovascular structures were obscured by fluorescein dye leakage and staining of the surrounding tissue. Time points following the intravenous injection of fluorescein were for NaCl, aflibercept and AF564 10.19 seconds, 09.09 seconds, and 10.08 seconds, respectively. For histology, endothelial cells in flat mounts were stained with isolectin B4 (last column, D21).

Fig. 2) was possible in the NaCl (Supplementary Fig. S3), aflibercept (Supplementary Fig. S4), and AF564 (Supplementary Fig. S5) treatment group for all tested days and layers in OCTA images. Immediately following the initial laser treatment, signs of edema were visible at the site of the laser spots surrounded by normal retinal and choroidal vessel structures. The swelling was localized in and around the laser lesions and was especially visible at D2. First signs of neovascular structures were detectable 7 days following laser treatment in the DVP, ONL, EZ, as well as IC and OC in the NaCl (Supplementary Fig. S3), aflibercept (Supplementary Fig. S4), and AF564 (Supplementary Fig. S5) treatment groups.

The occurrence of early CNV formation was observed particularly in the DVP, ONL, and EZ with continued development in structure, size, and number of new blood vessels until day 21 (see Fig. 2). Particular in the ONL and EZ of (NaCl) control eyes, a subtle neovascular capillary network was visible in OCTA images at days 14 and 21 compared to VEGF inhibitor treated eyes (see Fig. 2). In the aflibercept and AF564 treatment groups, signs of neovascular vessels were also identified in the ONL, whereas a different pattern

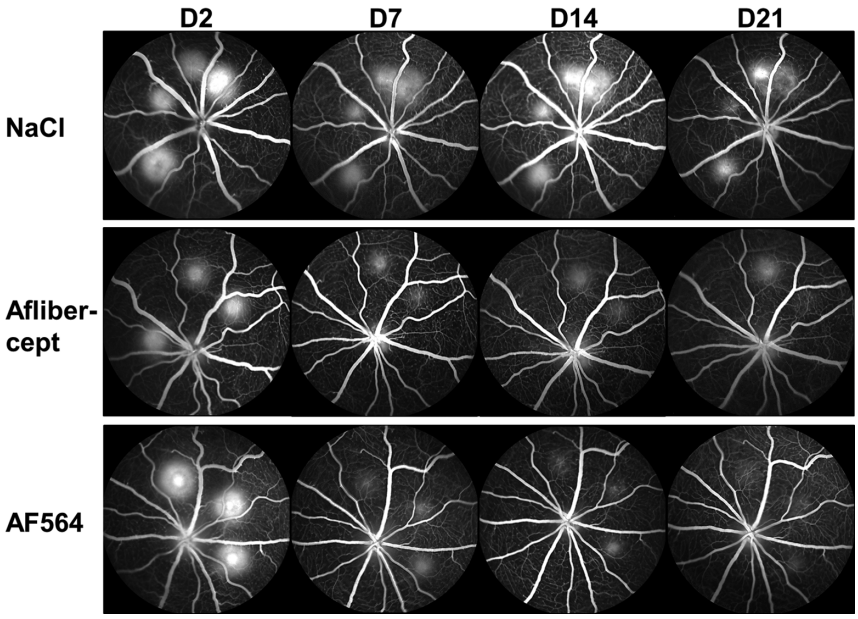

Figure 3. Rat fundus imaging by FA over time. Representative FA images are shown approximately 2 to 4 minutes after the intravenous application of fluorescein. The dye distribution and leakages are shown 2, 7, 14, and 21 days after laser treatment for NaCl (*first row*), aflibercept (*middle row*), and AF564 (*last row*) treated eyes (abbreviation: D = day following laser treatment). Overall, a decrease in fluorescence area and intensity was observed in all treatment groups over time. In addition, the treatment group aflibercept and AF564 showed less intense leakage compared to the control group NaCl, which is particularly evident at D21.

was observed in the EZ (see Fig. 2). Here, a roundish area in the form of a hyper-reflective plaque developed over time, which was particular detectable at D14 and D21 in OCTA but not in FA images. This pattern was detectable in 95% in aflibercept, 97% in AF564, and 7% in NaCl treated eyes. In general, no distinct changes or vessel formation were observed in the SVP and in the IVP only marginal changes were detected for all treatment groups at all time points (Supplementary Figs. S3, S4, S5, and S6). Overall, some projection artifacts of the main superficial retinal vessels were noted in OCTA in almost all deeper layers like IVP, DVP, ONL, EZ, and the IC (see Fig. 2 and Supplementary Figs. S3, S4, and S5).

Representative images of FA are shown approximately 2 to 3 minutes after intravenous application of fluorescein in Figures 2 and 3. With FA, the vascular network of the eye was imaged confocal using the cSLO technique, which allowed for monitoring of fluorescein leakage at the CNV site in vivo (see Fig. 3). At the same time, the dye leakage obscured the detailed structure of the neovascular capillary network in the retina and choroid, whereas anti-VEGF treatment effects became still visible over time regarding the fluorescence intensity and area (Supplementary Figs. S2, S3, S4, and S5). In the NaCl control group, leakage was detectable at day 2 following the initial laser treatment in all retinal and choroidal layers with a decrease in intensity, structure and size until day 21 (see Fig. 3). Qualitative evaluation of images revealed a noticeable reduction of the lesion sizes as well as dye leakage (see Fig. 3) in aflibercept and AF564 treated eyes over time as compared to the NaCl control group (same day and layer). In addition, some but not all lesions in the aflibercept and AF564 treatment groups were barely visible and showed no hyperfluorescence or leakage anymore (see Fig. 3). Furthermore, the treatment groups aflibercept and AF564 showed less intense leakages compared with the control group NaCl, which was particularly evident at D21 (see Figs. 2 and 3).

Quantitative Analysis of Laser-Induced CNV

The quantitative evaluation revealed that measured values of the CNV area were largest for the OC in FA images and for the EZ in OCTA images 2 days following the initial laser treatment (Supplementary Figs. S6 and S7). Subsequently, for both imaging modalities the lesion size decreased over time for all treatment groups (Figs. 4 and 5). This regression of CNV size was observed in OCTA images particularly in the DVP, ONL, EZ, IC, and OC, whereas in FA images all layers were affected (see Fig. 5). In general, a relative

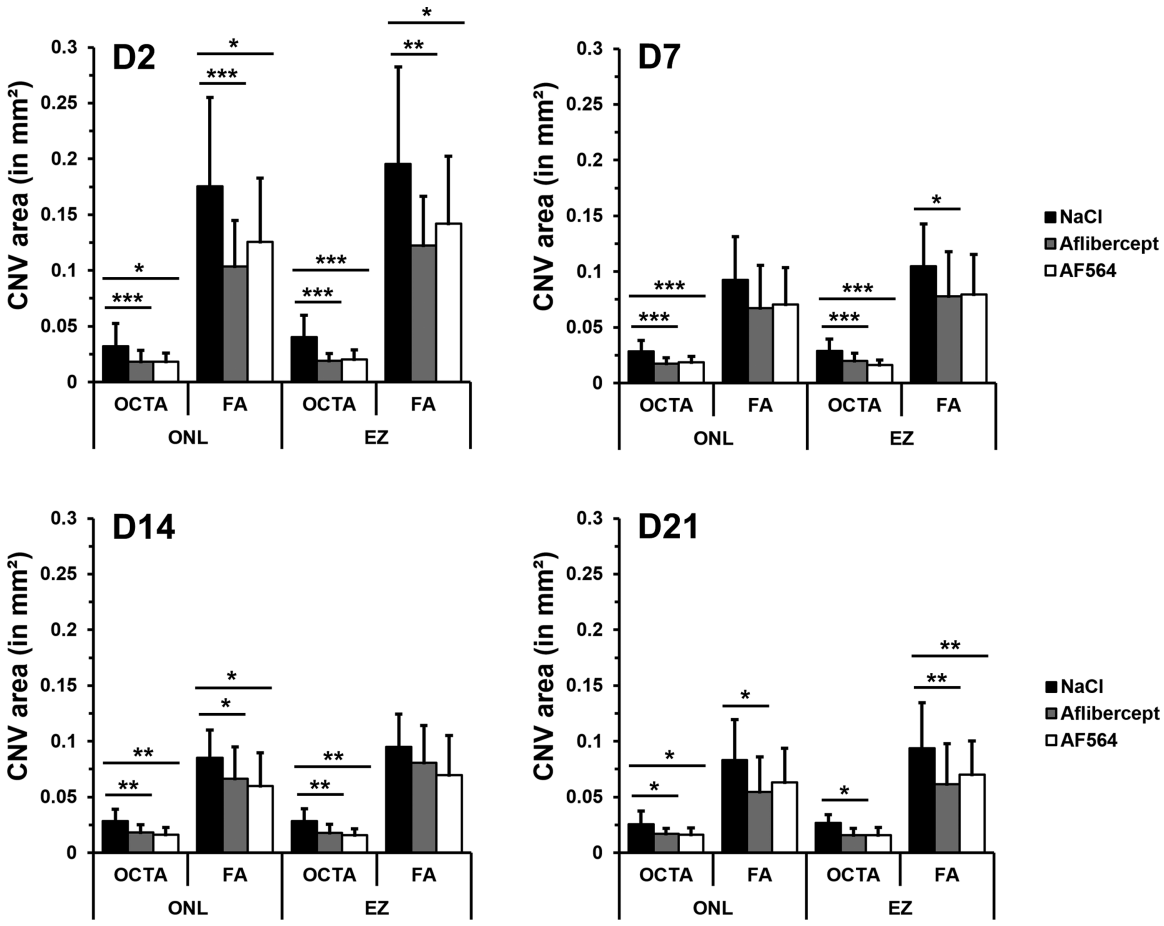

Figure 4. Assessment of the CNV area (in mm^2) for ONL and EZ in OCTA and FA at different time points. In each graph, the columns for the three different treatment groups (NaCl: $n = 30$ laser spots, aflibercept: $n = 19$, and AF564: $n = 37$) are highlighted by the same different grey values, respectively. Due to leakage and staining effects, the CNV area in the ONL and EZ was significantly larger in FA compared to OCTA images for all time points. CNV area size peaked at D2 in both image modalities and an overall less CNV development in the ONL and EZ was measured following the treatment with aflibercept and AF564 as compared to NaCl. In addition, size of the CNV area decreased over time in all treatment groups (* $P \leq 0.05$; ** $P \leq 0.01$; *** $P \leq 0.001$, Wilcoxon test comparing the CNV area in NaCl, aflibercept, and AF564 treated eyes in OCTA and FA images).

smaller CNV area was found in OCTA as compared to FA (about twice or even three times larger, all days and treatment groups; $P \leq 0.0001$, Supplementary Figs. S6 and S7). The decrease in the laser lesion size was overall stronger in FA compared to OCTA images (see Fig. 5). Of note, the size of the laser spots in the NaCl control group decreased in both image modalities to a lesser extent compared to the aflibercept and AF564 treatment groups (see Fig. 5). The CNV area was determined for the ONL and the EZ in more detail and the largest laser spots were observed at D2 (see Fig. 4). Comparing the area size of CNV lesions among groups, both OCTA and FA imaging revealed significantly smaller lesions for aflibercept and AF564 as compared with controls at all time points (see Fig. 4). No significant difference between aflibercept and AF564 treated eyes in OCTA or in FA images was detected (see Fig. 4). In addition, the change in the laser spot size reached a plateau at D14 in the AF564 treatment group and then changed only slightly, whereas the reduction in the aflibercept treatment group continued until D21 (see Fig. 5). Overall, the reduction of CNV size at D21 reached similar levels for aflibercept and AF564 in OCTA and FA images.

Grading Score and Pixel Intensity

Significant fluorescein leakage (defined as grade 3 lesions) was observed in all treatment groups at D2 (see Fig. 6). In general, the proportion of grade 0 lesions (no leakage) increased for all treatment groups over time while the proportion of grade 3 lesions decreased (see Fig. 6 and Supplementary Fig. S8). In total, at D21 (Fig. 6B) the amount of the grade

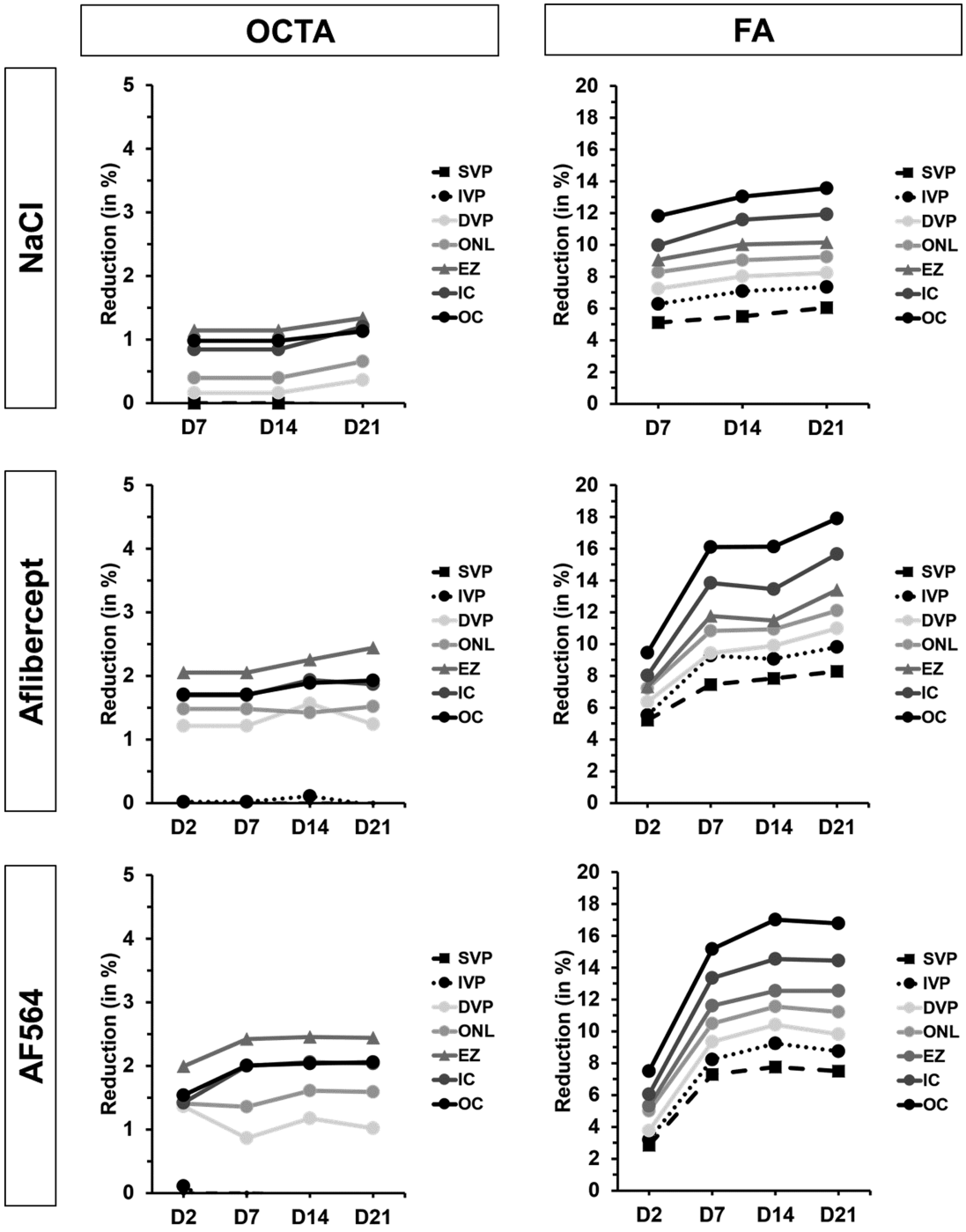

Figure 5. Reduction of the CNV area over time. The reduction of the CNV area for OCTA and FA images was determined with respect to the size of the laser lesions at D2 of the NaCl control group. In general, the decrease in the laser lesion size was overall greater in FA compared to OCTA images. In addition, in OCTA and FA images, the CNV area decreased only slightly in the NaCl control group over time and a larger regression was observed in the aflibercept and AF564 group.

3 lesions in the anti-VEGF treatment groups aflibercept (0%) and AF564 (2.6%) was significantly less ($P = 0.031$) compared with the NaCl control group (21%). In addition, the level of grade 0 lesions was highest for the aflibercept group (47%) compared to the AF564 (29%) and NaCl (8%) treatment groups, respectively (see Fig. 6B).

The mean pixel intensity within laser lesions was examined and the background fluorescence as well as the mean gray value was subtracted to determine the

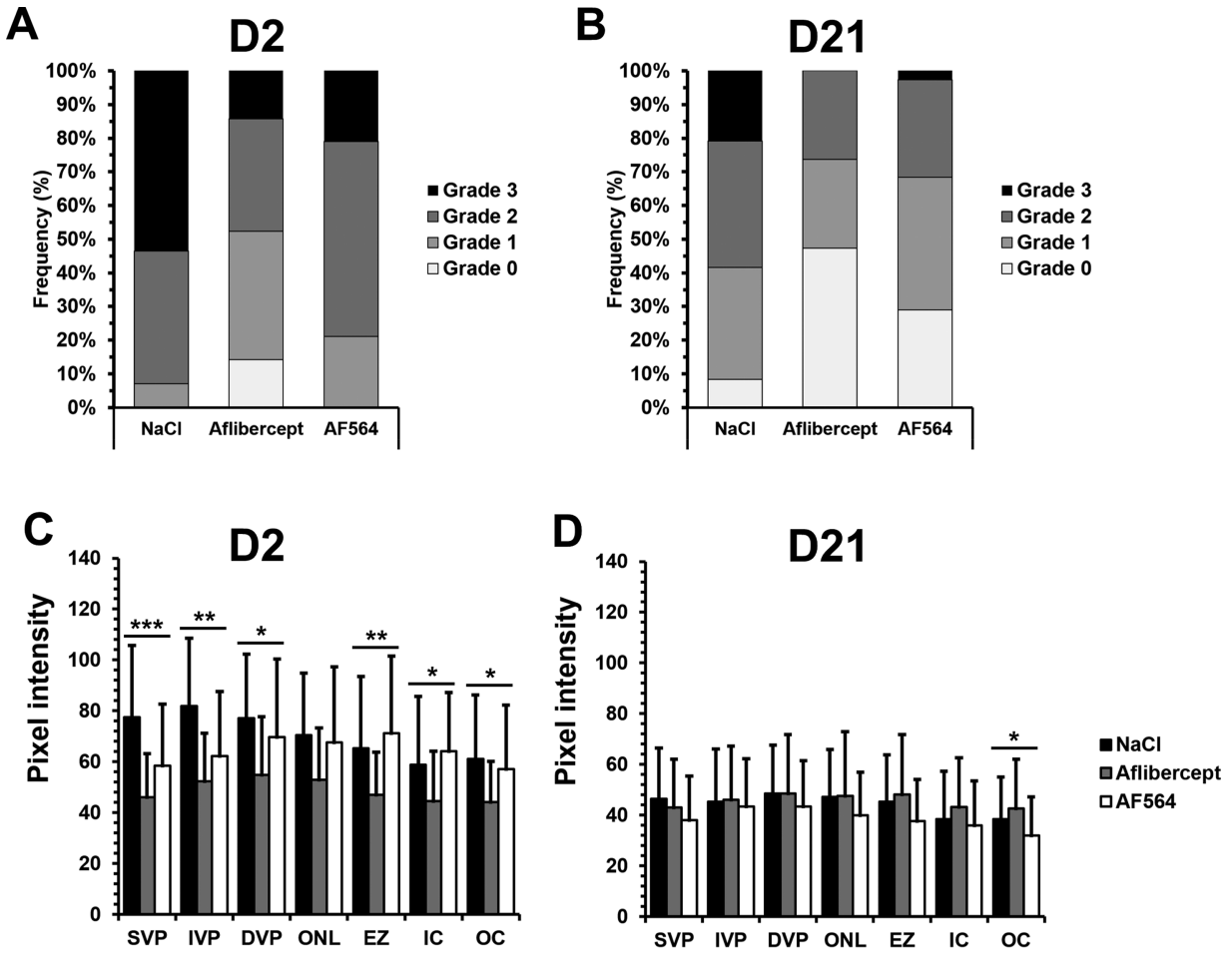

Figure 6. Grading score and mean pixel intensity of laser lesions in FA images. Histogram of angiographic leakage grades are shown in (**A**) (D2) and (**B**) (D21). The proportion of grade 0 lesions increased for all groups while the proportion of grade 3 lesions decreased significantly (comparison D2 to D21: $P = 0.031$) over time. Overall, a decrease in pixel intensity was observed from D2 (**C**) until D21 (**D**). In addition, the treatment group aflibercept and AF564 showed significant less intense leakages compared to the control group NaCl at D2 (shown by * $P \leq 0.05$; ** $P \leq 0.01$; and *** $P \leq 0.001$). Aflibercept treated eyes showed a reduced pixel intensity in the laser lesions at D2, whereas AF564 treated eyes showed less pixel intensity at D21 compared to NaCl.

laser lesion pixel intensity (Figs. 6C, 6D and Supplementary Fig. S8). Overall, the laser spots at D21 (see Fig. 6D) showed a reduced pixel intensity compared to D2 and the lowest pixel intensity within the laser lesions were determined for AF564 treated eyes (D21: SVP, IVP, DVP, and IC: not significantly different; ONL: $P = 0.034$ and OC: $P = 0.004$).

Retinal Vascular Network Structure Assessment

The vessel density (Fig. 7A) and number of vessel junctions (Fig. 7B) of SVP, IVP, and DVP in OCTA and FA images for the different treatment groups was evaluated within the laser spots over time (Supplementary Fig. S9) using AngioTool. An exemplary AngioTool output is shown in Figure 7D in which the outline of the vessels is indicated in yellow, the skeleton in red, and the branching points in blue. Analysis of the mean vessel density (as the ratio of percentage of vessels and total area) and number of vessel junctions between OCTA and FA showed similar results for the SVP for the three treatment groups as well as imaging method and no significant difference was found. In total, the vessel density as well as the number of vessel junctions showed an increase from SVP to IVP to DVP in OCTA images (see Figs. 7A, 7B). This effect was also detected to a lesser extent in FA images. Furthermore, an increase in vessel density and number of vessel junctions in deeper layers (IVP and DVP) in OCTA compared with FA images was determined for NaCl, aflibercept, and AF564. Statistical analysis using the Wilcoxon test showed significance higher vessel density

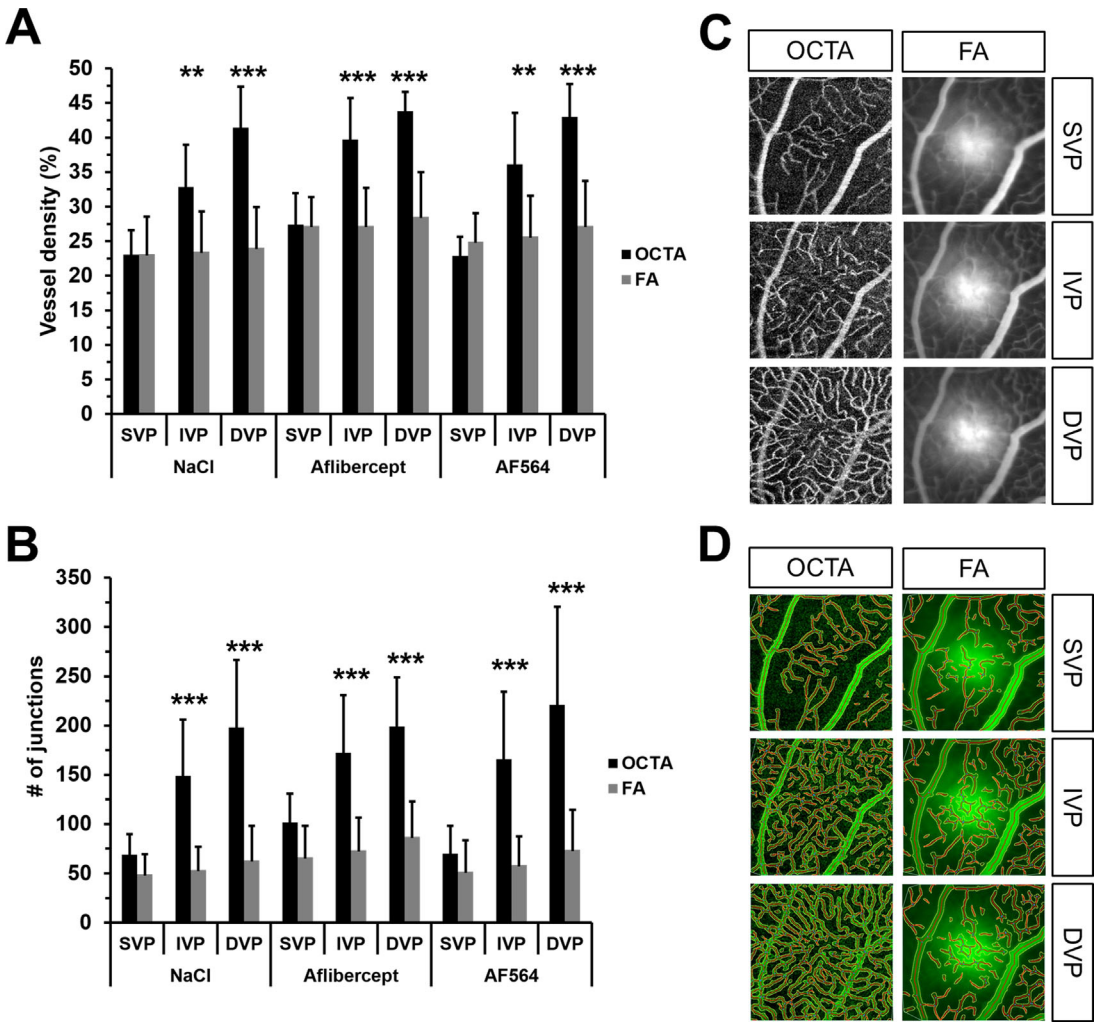

Figure 7. Analysis of the vessel density and number of vessel junctions. The mean vessel density (**A**) and the number of vessel junctions (**B**) were measured separately for the three retinal vascular plexus SVP, IVP, and DVP in the laser spot area in NaCl ($n = 30$), aflibercept ($n = 19$), and AF564 ($n = 37$) treated eyes for OCTA and FA 21 days (D21) following the laser treatment (example in **C** for the NaCl treatment group at D21). Analysis of the mean vessel density (as the ratio of percentage of vessels and total area) and number of vessel junctions between OCTA and FA, shown similar results for the SVP for the three different treatment groups as well as imaging method and no significant difference was found. Statistical analysis using the Wilcoxon test showed significance higher vessel density and number of vessel junctions at D21 between OCTA and FA for the IVP and DVP in all treatment groups (shown by ** $P \leq 0.01$; *** $P \leq 0.001$). The AngioTool output of OCTA and FA images **C** is shown in the corresponding lower column **D**, in which the outline of the vessels is indicated in *yellow*, the skeleton in *red*, and the branching points in *blue*.

and number of vessel junctions at D21 between OCTA and FA for the IVP (vessel density: $P \leq 0.01$; number of vessel junctions: $P \leq 0.0001$) and DVP (vessel density and number of vessel junctions: $P \leq 0.0001$) in all three treatment groups (see Figs. 7A, 7B). In general, there was a good agreement between the original OCTA images and the overlay of the AngioTool output, whereas in FA images, dye leakage covered the neovascular complex especially in the IVP and DVP resulting in a poor correlation with the software output (Figs. 7C, 7D).

Histology

Immunohistochemistry on retinal and RPE/choroidal/scleral flat mounts was performed 21 days following initial laser treatment (see Fig. 8). Ex vivo analysis and immunohistochemical staining of the flat mounts with isolectin B4 showed new vessel formation within the center of laser lesions in all three treatment groups but particularly in NaCl treated eyes. Clear neovascular vessel formation was detected in the retinal flat mounts in the region comparable to the

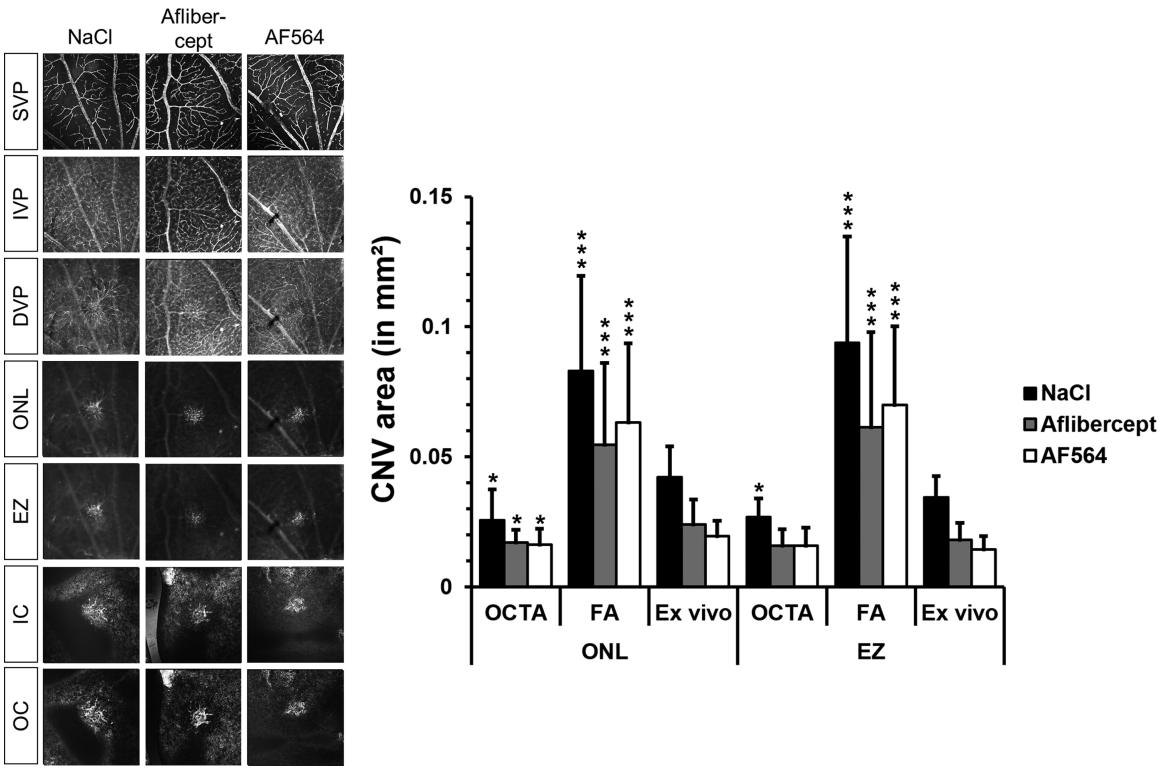

Figure 8. Laser lesions imaging by confocal microscopy. Ex vivo imaging by confocal microscopy (example of NaCl, aflibercept and AF564) of retinal as well as RPE/choroidal/scleral flat mount preparations for the different retinal and choroidal layers at day 21 following the initial laser treatment. For histology, endothelial cells in flat mounts were stained with isolectin B4 and the area of CNV (in mm^2) for OCTA, FA and confocal microscopy (ex vivo) images of retinal as well as RPE/choroidal/scleral flat mount preparations were calculated (for D21). Overall, CNV area in flat mounts was similar to OCTA results and smaller compared to area of dye leakage by FA for all treatment groups indicating the higher resolution achieved by OCTA. Comparison of mean CNV area between OCTA and histology for NaCl, aflibercept and AF564 in the ONL and EZ or FA and histology for NaCl, aflibercept, and AF564 in the ONL and EZ were performed with the Wilcoxon test (* $P \leq 0.05$; ** $P \leq 0.01$; *** $P \leq 0.001$, Wilcoxon test, OCTA and FA results were compared to ex vivo results, respectively).

DVP, ONL, and EZ for all tested treatment groups (see Fig. 8). In addition, in vivo OCTA and FA results were correlated with confocal microscopy images of the retinal and RPE/choroidal/scleral flat mounts of the different treatment groups and the CNV area of all three imaging modalities was calculated for the ONL and EZ (see Fig. 8). Almost no sign of neovascular vessel formation was detected in the ex vivo preparations for the SVP and only a minor area was affected in the IVP. These findings were comparable to the OCTA results (Figs. 3, 8). The CNV area was largest in the ONL in retinal flat mounts in NaCl treated eyes and smallest in the ONL as well as EZ for eyes treated with AF564 (see Fig. 8). Overall, the area of CNV in retinal and RPE/choroidal/scleral flat mounts was similar to OCTA results and significant smaller compared to the area of dye leakage by FA (OCTA versus histology = NaCl: ONL: $P = 0.012$, EZ: $P = 0.02$; aflibercept: ONL: $P = 0.04$, EZ: not significantly different; AF564: ONL: $P = 0.033$, EZ: not significantly different; FA versus histology: for all NaCl, aflibercept, and AF564 in the ONL and EZ: $P \leq 0.0001$). The significant differences were calculated using the Wilcoxon test and particularly evident in ONL compared to EZ (see Fig. 8).

Discussion

The results of our study indicate that in vivo OCTA imaging allows for precise and detailed evaluation of both CNV development and subsequent longitudinal evaluation of therapeutic effects of two different anti-VEGF inhibitors in the laser-induced CNV animal model. The selective visualization of neovascular vessels in the physiologically avascular outer retinal layer initially, followed by substantial

decrease of laser lesion size and vessel morphology as compared to the control group over time is in accordance with the current knowledge of CNV development and treatment effects of anti-VEGF agents, as previously shown in the rodent model of laser-induced CNV and in patients with CNV in the presence of various degenerative retinal-choroidal diseases, including AMD.[20,21,38–41] Furthermore, the direct correlation of in vivo findings by ex vivo analysis in the same animal further confirms these observations, also revealing consistent results with regard to quantification of individual lesion size.

Beyond the obvious benefit of a noninvasive imaging modality, OCTA showed several additional advantages when compared to FA, which has been considered standard imaging modality for CNV imaging in the rodent model up to now. First, the detailed and high-contrast visualization of the new vascular network by OCTA underlines the higher axial resolution and more accurate three-dimensional localization of vascular structures. Due to leakage effects and the limited axial resolution, FA did not allow for an accurate visualization of CNV progression in the ONL and EZ which are well-known to be the primary retinal layers for CNV development. Second, the observation of a roundish area in form of a hyper-reflective plaque by OCTA, which was not detectable by FA in the later course of the longitudinal monitoring in the two anti-VEGF treatment groups, indicates early formation of atrophy and fibrotic tissue. This assumption would be also in accordance with observations in patients with AMD that develop fibrosis and hyper-reflective material at the level of the outer retina, following treatment with repetitive anti-VEGF injections. An obvious limitation of OCTA as compared to FA was the inability to demonstrate leakage effects of CNV development and the further reduction of leakage at the site of laser lesions over time. The more pronounced reduction in FA leakage in aflibercept and AF564 treatment groups as compared with the controls also allowed for monitoring therapeutic effects of the anti-VEGF agents, which clearly confirms previous reports.[21] We believe that both imaging modalities offer the opportunity to study different aspects of CNV development and treatment response. One technique should not replace the other, they rather potentially complement each other in order to expand the insight into the pathophysiology of neovascular lesion in animal models and blinding retinal diseases.[22]

Comparing treatment effects between aflibercept and AF564 treated eyes, no obvious differences were seen with regard to development and regression of both CNV area and morphology. The only difference was related to an earlier reduction of laser spot size, as determined by FA, following AF564 intervention, reaching a plateau at D14. By contrast, aflibercept treatment resulted in a reduction of laser spot size until D21. This observation, which could not be determined by OCTA, may indicate that AF564 inhibit VEGF more effectively than aflibercept in the applied animal model of laser-induced CNV. Another explanation may be the interindividual variability in treatment responses between different animals or other confounders in the experimental setting, which may have caused this minor effect.

Limitations of the current study include the investigation of not more than three different agents or the application of agents. At the same time, we are confident that we could demonstrate clear differences between the treatment groups, which are in accordance with previous research. One strength of the study includes the superior image quality of OCTA using a commercial available system that was an important perquisite for the precise qualitative and quantitative analysis.[22] Careful anesthesia of the animals allowed reducing motion artifacts and also longer imaging sessions taking advantage of averaging of multiple image frames in order to enhance the signal-to-noise ratio. A potential improvement of the system could be the enlargement of the currently limited scan field and, thus, cover several lesions in one image. Due to the noninvasive method, information of dye leakage or staining are not detectable by OCTA. Nevertheless, dye leakage in FA clearly reveal the area of laser lesions and is a useful as well as worldwide established tool for drug treatment investigations.[22] On the other hand, OCTA images of the posterior pole can be generated in high quality even in the laser-induced CNV animal model, which could provide new insights in the longitudinal development of CNV. It should also be noted that the pathophysiological mechanism of the animal model differs from neovascular AMD in humans. For example, rodents have no macular and there is no accumulation of lipofuscin or drusen formation.

In conclusion, we demonstrated the feasibility of longitudinal and noninvasive in vivo OCTA monitoring in the rat model laser-induced CNV. In addition, therapeutic effects of anti-VEGF inhibitors (aflibercept and AF564) were monitored in vivo by combined OCTA and FA imaging. Detailed and high-contrast images of the retinal and choroidal vasculature in the center of the induced laser lesions were accurately visualized in vivo and over time by OCTA, which was not detectable by FA. Particularly, the avascular zone of ONL and EZ was visualized more in detail by OCTA. The direct in vivo visualization of the CNV microvasculature by OCTA may provide

more information and could enable an overall better understanding of pathophysiological changes as well as pharmaceutical interventions during CNV formation and progression.

Acknowledgments

The authors thank the Microscopy Core Facility of the Faculty of Medicine and the Institute for Medical Biometry, Informatics, and Epidemiology for statistical support at the University of Bonn, in particular Hannes Beckert and Rolf Fimmers. Technical support for OCTA imaging was provided by Heidelberg Engineering GmbH.

Supported by the Dr. Gaide-AMD Award 2017 (J.H.M.). No sponsor or funding agency had any involvement in the design, collection, analysis, and interpretation of the data, manuscript writing, and the decision to submit the manuscript for publication.

Portions of these data have been presented at the Association for Research in Vision and Ophthalmology Annual Meeting in 2018 and 2019.

Disclosure: **J.H. Meyer**, None; **J. Marx**, None; **C. Strack**, None; **F.G. Holz**, Acucela (C, F, R), Allergan (F, R), Apellis (C, R), Bayer (C, F, R), Boehringer-Ingelheim (C), Bioeq/Formycon (F, C), CenterVue (F), Ellex (R), Roche/Genentech (C, F, R), Geuder (C), Grayburg Vision (C, R), Heidelberg Engineering (C, F, R), Kanghong (C, F), LinBioscience (C, R), NightStarX (F), Novartis (C, F, R), Optos (F), Pixium Vision (C, F, R), Oxurion (C, R), Stealth BioTherapeutics (C, R), Zeiss (F, R); **S. Schmitz-Valckenberg**, Acucela (F), Alcon/Novartis (C, F, R), Allergan (C, F, R), Bayer (F, R), Bioeq/Formycon (F, C), Carl Zeiss MedicTec (F, R), CenterVue (F), Galimedix (C), Genentech/Roche (F, R), Heidelberg Engineering (F), Katairo (F), Optos (F)

References

1. Lim LS, Mitchell P, Seddon JM, Holz FG, Wong TY. Age-related macular degeneration. *Lancet*. 2012;379:1728–1738.
2. Ferrara N, Kerbel RS. Angiogenesis as a therapeutic target. *Nature*. 2005;438:967–974.
3. Ferrara N. Vascular endothelial growth factor and age-related macular degeneration: from basic science to therapy. *Nat Med*. 2010;16:1107–1111.
4. Rosenfeld PJ, Brown DM, Heier JS, et al. Ranibizumab for neovascular age-related macular degeneration. *N Engl J Med*. 2006;355:1419–1431.
5. Martin DF, Maguire MG, Fine SL, et al. Ranibizumab and bevacizumab for treatment of neovascular age-related macular degeneration: two-year results. *Ophthalmology*. 2012;119:1388–1398.
6. Heier JS, Brown DM, Chong V, et al. Intravitreal aflibercept (VEGF trap-eye) in wet age-related macular degeneration. *Ophthalmology*. 2012;119:2537–2548.
7. Nguyen QD, Das A, Do DV, et al. Brolucizumab: evolution through preclinical and clinical studies and the implications for the management of neovascular age-related macular degeneration. *Ophthalmology*. 2020;17:30041–30045.
8. Yang S, Zhao J, Sun X. Resistance to anti-VEGF therapy in neovascular age-related macular degeneration: a comprehensive review. *Drug Des Devel Ther*. 2016;10:1857–1867.
9. Bhisitkul RB, Desai SJ, Boyer DS, Sadda SR, Zhang K. Fellow eye comparisons for 7-year outcomes in ranibizumab-treated AMD subjects from ANCHOR, MARINA, and HORIZON (SEVEN-UP Study). *Ophthalmology*. 2016;123:1269–1277.
10. Jia Y, Morrison JC, Tokayer J, et al. Quantitative OCT angiography of optic nerve head blood flow. *Biomed Opt Express*. 2012;3:3127–3137.
11. Jia Y, Bailey ST, Wilson DJ, et al. Quantitative optical coherence tomography angiography of choroidal neovascularization in age-related macular degeneration. *Ophthalmology*. 2014;121:1435–1444.
12. Chalam KV, Sambhav K. Optical coherence tomography angiography in retinal diseases. *J Ophthalmic Vis Res*. 2016;11:84–92.
13. Spaide RF, Fujimoto JG, Waheed NK, Sadda SR, Staurenghi G. Optical coherence tomography angiography. *Prog Retin Eye Res*. 2018;64:1–55.
14. Giani A, Thanos A, Roh MI, et al. In vivo evaluation of laser-induced choroidal neovascularization using spectral-domain optical coherence tomography. *Invest Ophthalmol Vis Sci*. 2011;52:3880–3887.
15. Cunea A, Meyer J, Russmann C, et al. In vivo imaging with a fundus camera in a rat model of laser-induced choroidal neovascularization. *Ophthalmologica*. 2014;231:117–123.
16. Hoerster R, Muether PS, Vierkotten S, Schroder S, Kirchhof B, Fauser S. In-vivo and ex-vivo characterization of laser-induced choroidal neovascularization variability in mice. *Graefes Arch Clin Exp Ophthalmol*. 2012;250:1579–1586.

17. Giannakaki-Zimmermann H, Kokona D, Wolf S, Ebneter A, Zinkernagel MS. Optical coherence tomography angiography in mice: comparison with confocal scanning laser microscopy and fluorescein angiography. *Transl Vis Sci Technol*. 2016;5:11.
18. Uehara H, Lesuma T, Stocking P, et al. Detection of microvascular retinal changes in type I diabetic mice with optical coherence tomography angiography. *Exp Eye Res*. 2018;27:30516–30515.
19. Shah RS, Soetikno BT, Yi J, et al. Visible-light optical coherence tomography angiography for monitoring laser-induced choroidal neovascularization in mice. *Invest Ophthalmol Vis Sci*. 2016;57:OCT86–OCT95.
20. Wang WQ, Wang FH, Qin WX, et al. Joint antiangiogenic effect of ATN-161 and anti-VEGF antibody in a rat model of early wet age-related macular degeneration. *Mol Pharm*. 2016;13:2881–2890.
21. Park JR, Choi W, Hong HK, et al. Imaging laser-induced choroidal neovascularization in the rodent retina using optical coherence tomography angiography. *Invest Ophthalmol Vis Sci*. 2016;57:OCT331–OCT40.
22. Meyer JH, Larsen PP, Strack C, et al. Optical coherence tomography angiography (OCT-A) in an animal model of laser-induced choroidal neovascularization. *Exp Eye Res*. 2019;184:162–171.
23. Nakagawa K, Yamada H, Mori H, Toyama K, Takahashi K. Comparison between optical coherence tomography angiography and immunolabeling for evaluation of laser-induced choroidal neovascularization. *PLoS One*. 2018;13:e0201958.
24. Meyer J, Cunea A, Sonntag-Bensch D, et al. In vivo imaging of a new indocyanine green micelle formulation in an animal model of laser-induced choroidal neovascularization. *Invest Ophthalmol Vis Sci*. 2014;55:6204–6212.
25. Dobi ET, Puliafito CA, Destro M. A new model of experimental choroidal neovascularization in the rat. *Arch Ophthalmol*. 1989;107:264–269.
26. Meyer JH, Cunea A, Licha K, et al. In vivo imaging of fluorescent probes linked to antibodies against human and rat vascular endothelial growth factor. *Invest Ophthalmol Vis Sci*. 2016;57:759–770.
27. Wang W, Wang F, Lu F, et al. The antiangiogenic effects of integrin alpha5beta1 inhibitor (ATN-161) in vitro and in vivo. *Invest Ophthalmol Vis Sci*. 2011;52:7213–7220.
28. Wigg JP, Zhang H, Yang D. A quantitative and standardized method for the evaluation of choroidal neovascularization using MICRON III fluorescein angiograms in rats. *PLoS One. 2015* 2015;10:e0128418.
29. McCloskey M, Wang H, Jiang Y, Smith GW, Strange J, Hartnett ME. Anti-VEGF antibody leads to later atypical intravitreous neovascularization and activation of angiogenic pathways in a rat model of retinopathy of prematurity. *Invest Ophthalmol Vis Sci*. 2013;54:2020–2026.
30. R&D S. Rat VEGF Antibody, AF564. 2020:Product information, https://www.rndsystems.com/products/rat-vegf-antibody_af564.
31. Meyer JH, Fang PP, Krohne TU, Harmening WM, Holz FG, Schmitz-Valckenberg S. [Optical coherence tomography angiography (OCTA) in rats]. *Ophthalmologe*. 2017;114:140–147.
32. Schmitz-Valckenberg S, Guo L, Maass A, et al. Real-time in vivo imaging of retinal cell apoptosis after laser exposure. *Invest Ophthalmol Vis Sci*. 2008;49:2773–2780.
33. Maass A, von Leithner PL, Luong V, et al. Assessment of rat and mouse RGC apoptosis imaging in vivo with different scanning laser ophthalmoscopes. *Curr Eye Res*. 2007;32:851–861.
34. Yu HG, Liu X, Kiss S, et al. Increased choroidal neovascularization following laser induction in mice lacking lysyl oxidase-like 1. *Invest Ophthalmol Vis Sci*. 2008;49:2599–2605.
35. Zhang P, Wang H, Luo X, et al. MicroRNA-155 inhibits polarization of macrophages to M2-type and suppresses choroidal neovascularization. *Inflammation*. 2018;41:143–153.
36. Zudaire E, Gambardella L, Kurcz C, Vermeren S. A computational tool for quantitative analysis of vascular networks. *PLoS One*. 2011;6:16.
37. von der Emde L, Thiele S, Pfau M, et al. Assessment of exudative activity of choroidal neovascularization in age-related macular degeneration by OCT angiography. *Ophthalmologica*. 2019;30:1–9.
38. Ferrara N, Adamis AP. Ten years of anti-vascular endothelial growth factor therapy. *Nat Rev Drug Discov*. 2016;15:385–403.
39. Balser C, Wolf A, Herb M, Langmann T. Co-inhibition of PGF and VEGF blocks their expression in mononuclear phagocytes and limits neovascularization and leakage in the murine retina. *J Neuroinflammation*. 2019;16:26.
40. Heiduschka P, Plagemann T, Li L, Alex AF, Eter N. Different effects of various anti-angiogenic treatments in an experimental mouse model of retinopathy of prematurity. *Clin Exp Ophthalmol*. 2019;47:79–87.
41. Krzystolik MG, Afshari MA, Adamis AP, et al. Prevention of experimental choroidal neovascularization with intravitreal anti-vascular endothelial growth factor antibody fragment. *Arch Ophthalmol*. 2002;120:338–346.